Molecular Catalysis 538 (2023) 113006

Contents lists available at ScienceDirect

Molecular Catalysis

journal homepage: www.journals.elsevier.com/molecular-catalysis

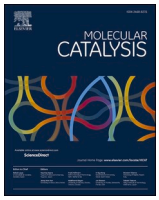

Manganese(III) complexes with tetradentate OˆCˆCˆO ligands: Synthesis, characterization and catalytic studies on the CO_2 cycloaddition with epoxides

Giammarco Meloni [a,b], Luca Beghetto [a], Marco Baron [a,b,*], Andrea Biffis [a,b], Paolo Sgarbossa [c], Miriam Mba [a], Paolo Centomo [a], Laura Orian [a], Claudia Graiff [d], Cristina Tubaro [a,b]

[a] Dipartimento di Scienze Chimiche, Università degli Studi di Padova, via Marzolo 1, 35131 Padova, Italy
[b] Consorzio Interuniversitario per le Reattività Chimiche e la Catalisi, Unità di Ricerca di Padova, via Marzolo 1, 35131 Padova, Italy
[c] Dipartimento di Ingegneria Industriale, Università degli Studi di Padova, via Marzolo 9, 35131 Padova, Italy
[d] Dipartimento di Scienze Chimiche, della Vita e della Sostenibilità Ambientale, Università degli Studi di Parma, Parco Area delle Scienze 17/A, 43124 Parma, Italy

ARTICLE INFO

Keywords:
Homogeneous catalysis
CO_2 chemical valorization
Phenolate ligands
Manganese organometallics
N-heterocyclic carbene

ABSTRACT

A novel class of manganese(III) complexes bearing bis(NHC)-bis(phenolate) (OˆCˆCˆO) type ligands was successfully synthesized. Three differently substituted imidazolium salts (with 2-hydroxyphenyl, **$(H_4L^1)Br_2$**, 5-tert-butyl-2-hydroxyphenyl, **$(H_4L^2)Br_2$**, and 3,5-di-tert-butyl-2-hydroxyphenyl, **$(H_4L^3)Br_2$**, groups) were prepared as precursors of the (OˆCˆCˆO) ligands and a convenient high-yield complexation reaction using manganese(III) acetate was developed. Electrospray ionization mass spectrometry (ESI-MS) and single-crystal X-ray diffraction (SC-XRD) data confirm the formation of the complexes of general formula **$[MnBrL^{1-3}]$** and clarify their coordination geometry. The complexes were studied as homogeneous catalysts in the cycloaddition of CO_2 to benzyl glycidyl ether (BGE) to form the corresponding cyclic carbonate, using tetrabutylammonium bromide (TBAB) or bis(triphenylphosphine)iminium bromide (PPNBr) as co-catalysts. The complex **$[MnBrL^3]$** shows the highest activity, and kinetic investigations revealed a pseudo-first order dependence with respect to BGE under neat conditions. The temperature effect was also investigated using the Eyring and Arrhenius equations and the activation parameters for the neat reaction using **$[MnBrL^3]$** and TBAB were experimentally determined ($\Delta H^{\ddagger}$ = 11.2 kcal·mol^{-1} and $\Delta S^{\ddagger}$ = -50 cal·mol^{-1}·K^{-1}). On the basis of the performed mechanistic studies and DFT investigations, a catalytic cycle which involves the CO_2 1,2-insertion as the rate determining step is proposed.

1. Introduction

Tetradentate bis(phenolate) ligands are documented in important pages of the coordination chemistry history. Their typical molecular scaffold consists of two phenolate donors (O) linked by a moiety that includes two neutral donors (D), forming a dianionic ligand (OˆDˆO). First reported in the 1930s by Paul Pfeiffer in their salen-type version (from salicylaldehyde (sal) and ethylenediamine (en)) [1], their most renowned applications are in the Mn(III) catalyzed asymmetric olefin epoxidation [2–4], and in group 4 metal complexes for olefin polymerization as post-metallocene systems [5]. Their metal complexes are usually very stable, due to the chelating effect. An array of three chelate rings is formed upon metal coordination, and the ligands can be classified according to the number of atoms forming the metallacyclic rings (e.g. 6–5–6 for salen). Over the years, different versions of these ligands were developed by changing the nature of the two neutral donors (D) between the phenolates (O). In particular, nitrogen (imine and amine) [6,7], thioether [8,9], and phosphine derivatives [10] were successfully reported (Fig. 1). More recently, a limited number of studies on their N-heterocyclic carbene (NHC) version appeared in the literature [11–13].

The presence of NHC donors in the ligand is very appealing, considering that they form very robust organometallic species. The main contribution in a NHC-M bond is the carbene σ-donation to the metal center; however, the π-contributions, either the back donation between the metal orbitals and the carbene p-orbital or the carbene π-donation, may not be negligible [14]. Moreover, the combination in a single ligand of soft (NHC) and hard (phenolate) donors is very intriguing, allowing in

* Corresponding author.
E-mail address: marco.baron@unipd.it (M. Baron).

https://doi.org/10.1016/j.mcat.2023.113006
Received 30 September 2022; Received in revised form 16 January 2023; Accepted 4 February 2023
Available online 15 February 2023

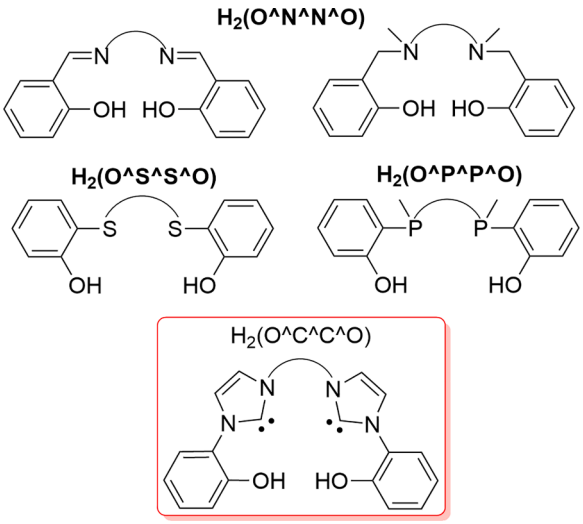

Fig. 1. Structures of tetradentate bis(phenolate) ligand precursors (H_2(O^D^D^O)) bearing N, S, and P (top) or NHC (bottom) neutral donors.

principle the formation of stable metal complexes with a wide variety of metal centers in different oxidation states [15]. A reason for the limited use of hybrid bis(NHC)-bis(phenolate) tetradentate ligands could be the lack of optimized synthetic procedures. Taking advantage of our established expertise in bis(NHC) chemistry [16–19], in this work we report a detailed study on the synthesis of three ligand precursors **(H_4L)Br_2**, aimed at facilitating the access to these compounds. The corresponding metal complexes can be obtained in a single step procedure without isolating the free ligand. As a proof of concept, we focused our efforts on the synthesis of Mn(III) complexes and used them as valuable catalysts in the synthesis of 1-benzylglycerol-2,3-carbonate from the corresponding epoxide and CO_2. Up to now, the reported examples of Mn(III) complexes with NHC ligands are very limited [11,20,21]. In fact, being NHCs soft donors, most of the studies regard Mn(I) NHC metal complexes [22–26]. Nevertheless, Mn(III) complexes have recently been shown to be particularly active homogeneous catalysts for the cycloaddition of CO_2 with epoxides [27–32]. The reaction between CO_2 and epoxides is an efficient route to prepare cyclic carbonates, and it is an effective way to perform a chemical valorization of CO_2, also at industrial level [33]. Important features, that make this reaction appealing, are (i) the use of a renewable, nontoxic and widely available reactant as carbon dioxide; (ii) the 100% atom efficiency and (iii) the possibility of running the synthesis under solventless conditions. The high free energy of epoxides provides the driving force to overcome the thermodynamic stability of carbon dioxide [34,35]. Several homogeneous and heterogeneous catalytic systems have been reported to be active in this transformation. Among the homogeneous systems the best performances have been obtained with metal complexes, both as bifunctional and binary systems [36–43]. Homogeneous metal catalysts are, in fact, used in combination with a nucleophile, typically a source of halide anions soluble in organic solvents, as co-catalyst [44]. Promising results have also been obtained by replacing metal complexes with organocatalysts, consisting of organic molecules acting as hydrogen-bond donors [45–47]. Moving toward heterogeneous catalysis, tailored bifunctional materials are indeed the most investigated systems, with particular regard to metallorganic frameworks (MOFs) [48–50] and porous organic polymers (POPs) [51]. Alternative reported approaches involve the use of hybrid organic-inorganic materials, e.g. silsesquioxanes functionalized with imidazolium groups and covalently grafted on a silica support [52].

Concerning our study, the three investigated ligands differ for the substituents on the phenolic rings, with **L^1** having no substituents, while **L^2** and **L^3** have, respectively, a tert-butyl group in para or two tert-butyl groups in ortho and para position relative to the phenolate function (Scheme 1). This study combines experimental and theoretical data, the latter based on DFT calculations, to evaluate the catalytic performance of the Mn(III) complexes and to obtain mechanistic insight on the reaction.

2. Experimental

2.1. Materials and methods

All manipulations, unless otherwise noted, were carried out in air and all the reactants and the solvents were obtained from commercial suppliers and used as received. 2,4-di-tert-butyl-o-anisidine **a3**, was prepared according to the literature procedure starting from 2,4-di-tert-butylphenol [12]. Compounds **b1–3, c1–3** and **($H_4L^{1–3}$)Br_2** are already described in the literature and were prepared by following modified literature procedures [11–13], described in the supporting information. The ^{1}H, ^{13}C and ^{31}P NMR spectra were recorded at 298 K on a Bruker Avance 300 MHz (7.05 T) operating at 300.1, 75.5 and 121.5 MHz, respectively. Chemical shifts are reported in parts per million and calibrated to the solvent residue. ^{1}H NMR signals are labeled as *s* = singlet, *d* = doublet, *t* = triplet, *q* = quartet, *sept* = septet and *m* = multiplet. ESI mass spectra were recorded on a Finnigan Thermo LCQ-Duo ESI mass spectrometer operating in positive ion mode; sample solutions were prepared by dissolving the compounds in methanol and were directly infused into the ESI source by a syringe pump at 8 μL/min flow rate. Elemental analyses were performed by the microanalytical laboratory of Chemical Sciences Department (University of Padova) with a Thermo Scientific FLASH 2000 elemental analyzer.

2.2. Synthesis of the manganese(III) complexes [MnBrL^1], [MnBrL^2] and [MnBrL^3]

Method A. Under inert atmosphere, triethylamine (0.31 mmol) was added to a suspension of the proligand (0.070 mmol), manganese(III) acetate dihydrate (0.090 mmol) and tetraethylammonium bromide (0.35 mmol) in 10 mL of methanol. The suspension was heated at 55 °C

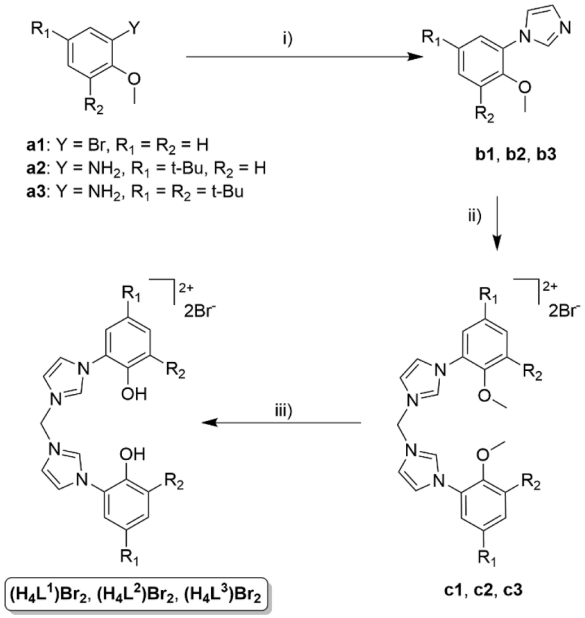

Scheme 1. Synthesis of ligand precursors **($H_4L^{1–3}$)Br_2**: i) *o*-bromoanisole, imidazole, KOH, CuO, 140 °C, 48 h, DMSO for **b1**, or 1) *o*-anisidine, glyoxal, NH_4Cl, H_2CO, H_3PO_4, reflux, EtOH/H_2O, 16 h and 2) KOH, H_2O for **b2** and **b3**; ii) CH_2Br_2, neat, 120 °C, 16 h; iii) HBr:HOAc 1:1 v/v, reflux, 48 h for **($H_4L^{1,2}$)Br_2** or BBr_3, DCM, 20 h, room temperature for **(H_4L^3)Br_2**.

for 16 h. The reaction mixture was then filtered at room temperature, and the filtrate was evaporated to dryness. The crude product was dissolved in dichloromethane (50 mL) and washed with distilled water (3 × 50 mL). The organic phase was then recovered and dried over $MgSO_4$. The drying agent was then removed by filtration, the solvent volume was subsequently reduced, and the solid product was precipitated with *n*-hexane, recovered by filtration and dried under vacuum.

Method B. Triethylamine (0.31 mmol) was added to a suspension of the proligand (0.070 mmol), manganese(II) acetate tetrahydrate (0.090 mmol) and tetraethylammonium bromide (0.35 mmol) in 10 mL of ethanol. The suspension was heated at 80 °C for 16 h. The product was then isolated by filtration, washed with cold ethanol, and dried under vacuum.

Method C. Under inert atmosphere, in a Schlenk tube, triethylamine (0.30 mmol) was added to a suspension of the proligand (0.10 mmol) and tetraethylammonium bromide (0.50 mmol) in ethanol (4 mL) (mixture A). In a second Schlenk tube, $Mn(acac)_3$ (0.10 mmol) was dissolved in 2 mL of ethanol (solution B). Solution B was then added dropwise to mixture A, and the resulting reaction mixture was heated at 75 °C for 4 h. The product was then isolated by filtration, washed with cold ethanol, and dried under vacuum.

The purity of the isolated complexes has been established by elemental analysis. Although the elemental analysis results are in a few cases outside the range viewed as establishing analytical purity, they are provided to illustrate the best values obtained to date.

[MnBrL^1] – Method A. Considering the low solubility of complex **[MnBrL^1]** in dichloromethane, the crude product was purified in this case by recrystallization from methanol/diethyl ether. Yield: 71%. Elemental analysis calcd (%) for $C_{19}H_{14}BrMnN_4O_2{\cdot}2CH_3OH{\cdot}H_2O$: C 46.09, H 4.42, N 10.24. Found: C 46.06, H 3.67, N 9.90. ESI(+)–MS (*m/z*): 384.99 $[MnL^1]^+$ measured for theoretical $C_{19}H_{14}MnN_4O_2^+$= 385.05, 800.82 $[(MnL^1)_2(MeOH)\text{-}H]^+$ measured for theoretical $C_{39}H_{31}Mn_2N_4O_5^+$= 801.12, 848.65 $[(MnL^1)_2(Br)]^+$ measured for theoretical $C_{38}H_{28}BrMn_2N_8O_4^+$= 849.02. Crystals suitable for SC-XRD analysis were obtained by slow diffusion of diethyl ether into a methanol solution of **[MnBrL^1]**.

[MnBrL^1] – Method B. Yield: 44%. Elemental analysis calcd (%) for $C_{19}H_{14}BrMnN_4O_2{\cdot}H_2O$: C 47.23, H 3.34, N 11.59. Found: C 47.12, H 3.45, N 11.14. ESI(+)–MS (*m/z*): 385.12 $[MnL^1]^+$ measured for theoretical $C_{19}H_{14}MnN_4O_2^+$= 385.05.

[MnBrL^1] – Method C. Yield: 49%. Elemental analysis calcd (%) for $C_{19}H_{14}BrMnN_4O_2{\cdot}H_2O{\cdot}EtOH$: C 47.66, H 4.19, N 10.59. Found: C 47.64, H 3.33, N 10.20. ESI(+)–MS (*m/z*): 385.00 $[MnL^1]^+$ measured for theoretical $C_{19}H_{14}MnN_4O_2^+$= 385.05, 800.86 $[(MnL^1)_2(MeOH)\text{-}H]^+$ measured for theoretical $C_{39}H_{31}Mn_2N_4O_5^+$= 801.12, 848.63 $[(MnL^1)_2(Br)]^+$ measured for theoretical $C_{38}H_{28}BrMn_2N_8O_4^+$= 849.02.

[MnBrL^2] – Method A. Yield: 95%. Elemental analysis calcd (%) for $C_{27}H_{30}BrMnN_4O_2{\cdot}½C_6H_{14}$: C 58.07, H 6.01, N 9.03. Found: C 58.16, H 5.81, N 9.18. ESI(+)–MS (*m/z*): 497.17 $[MnL^2]^+$ measured for theoretical $C_{27}H_{30}MnN_4O_2^+$= 497.17.

[MnBrL^3] – Method A. Yield: 83%. Elemental analysis calcd (%) for $C_{35}H_{46}BrMnN_4O_2$: C 60.96, H 6.72, N 8.12. Found: C 61.33, H 6.99, N 7.84. ESI(+)–MS (*m/z*): 609.25 $[MnL^3]^+$ measured for theoretical $C_{35}H_{46}MnN_4O_2^+$= 609.30, 1299.10 $[(MnL^3)_2(Br)]^+$ measured for theoretical $C_{70}H_{92}BrMn_2N_8O_4^+$= 1297.52. Crystals suitable for SC-XRD analysis were obtained by slow diffusion of hexane into an acetone solution of **[MnBrL^3]**.

2.3. X-ray structure determination of [MnBrL^1(MeOH)], [MnBrL^3] and [MnClL^3]

The crystallographic data for the two complexes were obtained by mounting a single crystal on a glass fiber and transferring it to an APEX II Bruker CCD diffractometer. The APEX 3 program package was used to obtain the unit-cell geometrical parameters and for the data collection (30 s/frame scan time for a sphere of diffraction data). The raw frame data were processed using SAINT and SADABS to obtain the data file of the reflections. The structures were solved using SHELXT [53] (Intrinsic Phasing method in the APEX 3 program). The refinement of the structures (based on F^2 by full-matrix least-squares techniques) was carried out using the SHELXTL-2014/7 [54] program in the Olex2 GUI [55]. The hydrogen atoms were introduced in the refinement in defined geometry and refined "riding" on the corresponding carbon atoms. Crystallographic data have been deposited with the Cambridge Crystallographic Data centre (CCDC 2155172–4 for complexes **[MnBrL^1(MeOH)]**, **[MnBrL^3]** and **[MnClL^3]**). Crystal data and refinement parameters are reported in Table S1.

2.4. General procedure for catalytic tests

Catalyst, co-catalyst, benzyl glycidyl ether (or the employed epoxide), the stirring bar and eventually the solvent were added into a 35 mL Fisher-Porter tube. The reactor was clapped and five cycles of pressurization/depressurization with CO_2 were performed (5 atm, unless otherwise stated in the text). The reactor was pressurized with CO_2 (5 atm, unless otherwise stated in the text) and dipped into a thermostatic bath. The stirring speed and immersion depth was maintained similar in all the performed tests. The starting time of the test was kept five minutes after the immersion in the thermostatic bath and the CO_2 pressure was maintained constant at initial value during the test. To stop the test, the reactor was removed from the thermostatic bath, depressurized, and cooled at room temperature using a water bath. A precise quantity of 2,5-dimethylfuran was added to the reactor and, after mixing the obtained solution, a small sample of the reaction mixture was transferred to an NMR tube and the ^{1}H NMR spectrum in $CDCl_3$ was registered. The yield of the reaction was determined via ^{1}H NMR, by using 2,5-dimethylfuran as internal standard. Every test was performed three times and the reported yield is the resulting average value. The yield obtained in the replication of the same test varied in the range ± 1%.

2.5. Computational details

Density Functional Theory (DFT) calculations were performed using the Amsterdam Density Functional (ADF) program [56–58]. The OPBE [59] density functional was used in combination with TZ2P basis set for all atoms. TZ2P is a large and uncontracted set of Slater-type orbitals (STOs), is of triple-z quality and was augmented with two sets of polarization functions on each atom. The frozen-core approximation was adopted for the core electrons: up to 1 s for C, N and O, and up to 2p in the case of Mn and up to 3p for Br, respectively. The zeroth-order regular approximation (ZORA) [60] was chosen to account for the scalar relativistic effects, as recommended in presence of heavy nuclei [61–64]. The numerical integration was performed using the Becke grid [65,66]. The ground state for all Mn species is a quintet; spin contamination was monitored and found in all cases negligible. This electronic state was assessed comparing optimized structures of [**MnBrL^1**] in triplet and quintet state. The latter was found more stable by 17.31 kcal mol^{-1}. Frequency calculations were run to check the nature of the optimized structures computed along the catalytic path: minima are characterized by all positive frequencies, while transition states have a single imaginary frequency which was analyzed and found associated to the correct vibration connecting the preceding minimum to the following product on the potential energy surface (PES).

3. Results and discussion

3.1. Synthesis and characterization

The synthesis of the ligand precursors **(H$_4$L$^{1–3}$)Br$_2$** is a multistep procedure that consists at least of three steps: *i*) synthesis of the 2-(imidazole-1-yl)anisole derivative (**b1–3**), starting from a 2-

bromoanisole or a 2-anisidine derivative; *ii*) formation of the corresponding bis(imidazolium) salt by introducing the methylene bridging group (**c1–3**) and *iii*) deprotection of the alcohol moieties (Scheme 1). In our work, precursors **a1** and **a2** are commercially available, whereas **a3** was prepared following literature procedures [12].

In all cases, the step with the lowest yield is the isolation of the imidazole derivative, and compounds **b1-b3** must be purified by column chromatography. In the second step, the obtainment of the bis(imidazolium) salts proceeds smoothly and almost quantitatively, in a reaction with a 100% atom economy. Finally, deprotection of the phenol groups can be performed by refluxing the **c** intermediates in a 1:1 (v/v) mixture of HBr and CH_3COOH, or by using BBr_3 at room temperature in CH_2Cl_2. When treating compound **c3** with the 1:1 (v/v) mixture of HBr and CH_3COOH, not only the deprotection of the phenol moieties occurs, but also the removal of the R_2 *t*-Bu groups. Therefore, any attempt to obtain **$(H_4L^3)Br_2$** using HBr failed, making the use of BBr_3 the only viable deprotection option. The formation of compounds **$(H_4L^{1-3})Br_2$** is confirmed by the presence of the phenolic protons signal at > 9.5 ppm in the ^1H NMR spectra and by the absence of the O—CH_3 signals in the ^1H and ^{13}C NMR spectra in DMSO-d_6.

The synthesis of the manganese(III) complexes **[MnBrL$^{1-3}$]** was carried out starting from the corresponding ligand precursors in a single step procedure, by using NEt_3 as base, NEt_4Br as bromide source, and methanol or ethanol as solvent, in the presence of a manganese precursor (Scheme 2). A bromide excess is necessary to drive the reaction towards the formation of the desired product and, particularly, to avoid bromide ligand scrambling (see further in the text). Complex **[MnBrL^2]** was already reported by Yagyu, Jitsukawa *et al.* [11], differently **[MnBrL^{1,3}]** were prepared for the first time in this work. In the synthesis of **[MnBrL^1]**, we tested three different manganese precursors, such as $Mn(OAc)_2 \cdot 4H_2O$, $Mn(OAc)_3 \cdot 2H_2O$ and $Mn(acac)_3$ (acac = acetylacetonate). The synthetic approach with $Mn(OAc)_2 \cdot 4H_2O$ is typically used in the synthesis of Mn(III) complexes with salen-type ligands [67], and is also the protocol followed by Yagyu, Jitsukawa *et al.* in the preparation of **[MnBrL^2]** [11]. The reaction with $Mn(OAc)_2 \cdot 4H_2O$ is carried out under air conditions, to allow the oxidation of Mn(II) to Mn(III). For the syntheses carried out using $Mn(OAc)_3 \cdot 2H_2O$ and $Mn(acac)_3$ as precursors, standard Schlenk techniques were used. All three precursors led to the formation of the desired Mn(III) complex but the highest yield was obtained using $Mn(OAc)_3 \cdot 2H_2O$. We thus decided to use this last precursor also in the synthesis of **[MnBrL^2]** and **[MnBrL^3]**. Complexes **[MnBrL$^{1-3}$]** were isolated as brown/orange solids. Complex **[MnBrL^1]** is soluble in polar organic solvents, such as DMSO and DMF, and sparingly soluble in MeOH and EtOH. Complexes **[MnBrL^{2,3}]**, bearing *t*-Bu substituents, are soluble in the same solvents as **[MnBrL^1]**, and are also well soluble in acetone and dichloromethane. Complexes **[MnBrL$^{1-3}$]** were characterized by elemental analysis, ESI-MS spectrometry and in the case of **[MnBrL^1]** and **[MnBrL^3]** also single crystal X-ray structure analysis. Moreover, the X-ray structure of **[MnClL^3]** was also solved (Figure S23). The latter species was likely formed in an attempt of purifying **[MnBrL^3]** via CH_2Cl_2/brine solvent extraction. Under these conditions the bromide substitution by a chloride rapidly occurs.

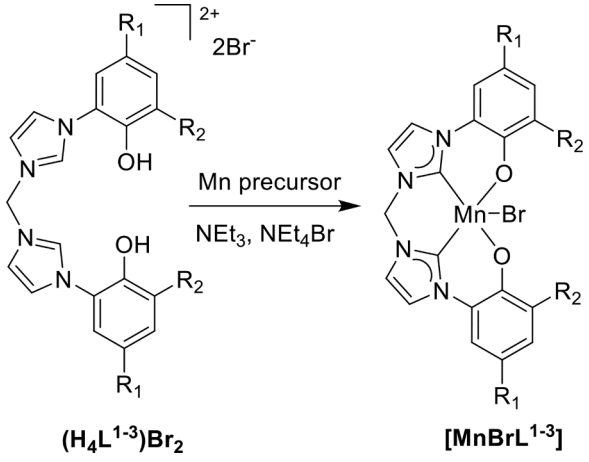

Scheme 2. Synthesis of the Mn(III) complexes **[MnBrL$^{1-3}$]**.

In the ESI-MS spectra of the manganese complexes, the presence as base peak of the signal related to the species $[MnL^{1-3}]^+$ at 384.99, 497.17, and 609.25 *m/z* for $[MnL^1]^+$, $[MnL^2]^+$, and $[MnL^3]^+$, respectively, is indicative of the coordination of the ligand to the Mn(III) center.

Crystals suitable for SC-XRD analysis were obtained by slow diffusion of diethyl ether into a methanol solution of **[MnBrL^1]**; conversely, crystals of **[MnBrL^3]** were obtained by slow diffusion of hexane into an acetone solution of the complex. The molecular structure present in the crystal obtained from the **[MnBrL^1]** solution belongs to the solvento complex **[MnBrL^1(MeOH)]**, that crystallizes in the P-1 space group. Complex **[MnBrL^1(MeOH)]** has a distorted octahedral coordination geometry, with the bis(NHC)-bis(phenolate) (**L^1**) ligand occupying the four square base positions, and a bromide and a methanol molecule in the two apical positions. The molecular structure of **[MnBrL^1(MeOH)]** together with selected bond distances and angles is shown in Fig. 2. The presence of the methanol coordinated to the Mn(III) center is probably due to the crystallization conditions. The Mn-OPh and Mn-C distances compare well to literature data [11]. The Mn-Br distance is considerably longer compared to **[MnBrL^2]** [11], and **[MnBrL^3]** (vide infra) because of the presence of the MeOH molecule in the *trans* position, and the resulting different coordination geometry. The Mn-Br bond length is rather similar to that observed in octahedral Mn(III) complexes with imine-phenolate or amine-phenolate ligands in which the same Br-Mn-$O_{(MeOH)}$ pattern is found [68]. In contrast, the Mn-$O_{(MeOH)}$ distance is longer than in the cited compounds [68], likely indicating that hexacoordination is less favored in the presence of the **L^1** ligand system. Complex **[MnBrL^1(MeOH)]** is the first example of a hexacoordinated Mn(III) complex with NHC ligands.

The molecular structure of **[MnBrL^3]** is shown in Fig. 3, together with selected bond distances and angles. Complex **[MnBrL^3]** crystallizes in the C2/c space group, together with a hexane solvent molecule. The complex presents a distorted square pyramidal coordination geometry, with the bis(NHC)-bis(phenolate) ligand (**L^3**) occupying the four square base positions and a bromide in the apical position. The Mn-

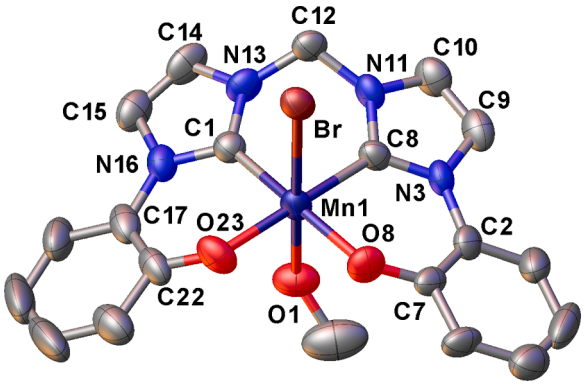

Fig. 2. ORTEP drawing of complex **[MnBrL^1(MeOH)]**. Ellipsoids are drawn at the 50% probability level. Hydrogen atoms and solvent molecules have been omitted for clarity. Selected bond distances (Å) and angles (°): Mn1-C1 2.008 (8), Mn1-C8 2.014(9), O8-Mn1 1.897(6), O23-Mn1 1.875(7), Mn1-Br 2.7351 (14), Mn1-O1 2.497(6), C1-Mn1-C8 86.2(4), O8-Mn1-C8 87.7(3), O23-Mn1-C1 87.7(3), O23-Mn1-O8 97.0(3), C1-Mn1-Br 92.1(2), C8-Mn1-Br 91.5(2), O8-Mn1-Br 96.63(19), O23-Mn1-Br 96.92(19), C1-Mn1-O1 80.7(3), C8-Mn1-O1 81.6(3), O8-Mn1-O1 89.9(3), O23-Mn1-O1 89.4(3), O8-Mn1-C1 169.4(3), O23-Mn1-C8 169.9(3), O1-Mn1-Br 170.28(14).

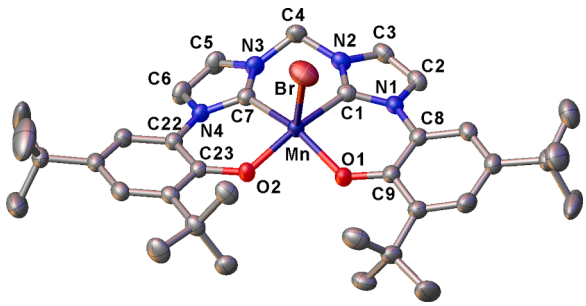

Fig. 3. ORTEP drawing of complex **[MnBrL^3]**. Ellipsoids are drawn at the 50% probability level. Hydrogen atoms and solvent molecules have been omitted for clarity. Selected bond distances (Å) and angles (°): C1-Mn 2.035(3), C7-Mn 2.036(3), Mn-O1 1.897(2), Mn-O2 1.880(2), Mn-Br 2.5324(6), C1-Mn-C7 86.48(12), O1-Mn-C1 86.06(11), O2-Mn-C7 86.61(10), O2-Mn-O1 90.71(9), C1-Mn-Br 94.80(8), C7-Mn-Br 106.61(8), O1-Mn-Br 104.32(7), O2-Mn-Br 104.14(7), O2-Mn-C1 160.99(11), O1-Mn-C7 148.66(11).

C, Mn-O and Mn-Br bond distances are in agreement with literature data [11]. The distortion in the coordination environment around the Mn center is highlighted by the difference in the C-Mn-Br angles that are 94.80(8) and 106.61(8) °, respectively for C1 and C7.

3.2. Catalytic studies

The catalytic activity of complexes **[MnBrL$^{1–3}$]** was studied toward the cycloaddition of benzyl glycidyl ether with CO_2 (Scheme 3). We selected benzyl glycidyl ether (BGE) as model substrate because of its low toxicity compared to other epoxides. Moreover BGE is also used to prepare poly(1,2-glycerol carbonate)s, a promising class of degradable polymers for biomedical and pharmaceutical applications [69–72].

A binary catalytic system was adopted using the Mn(III) complex and bis(triphenylphosphine)iminium bromide (PPNBr) or tetrabutylammonium bromide (TBAB) as co-catalyst. The ability of bromide salts with lipophilic cations to catalyze the cycloaddition of epoxides with CO_2 is well documented in the literature [44–47]. An initial screening of the reaction conditions was performed using DMF as solvent, to ensure a truly homogeneous system, and a CO_2 pressure of 5 atm (Table 1). In the absence of both the metal catalyst and the co-catalyst no product formation was observed in 19 h at 100 °C (Table 1, entry 1). No reaction was observed also using 1 mol% of PPNBr at 60 °C (Table 1, entry 2), whereas low yields of 1-benzylglycerol-2,3-carbonate were obtained in the presence of PPNBr or TBAB at 100 °C, working with 1 mol% or 0.1 mol% of the co-catalyst (Table 1, entries 3–5). By introducing catalyst **[MnBrL^1]** in the system (1 mol%), the desired product was obtained in traces at 25 °C, in moderate yield at 60 °C and in quantitative yield at 100 °C (3, 43 and 100% at 25, 60 and 100 °C, respectively; Table 1, entries 6–8). A quantitative yield is observed at 100 °C even working without the co-catalyst (Table 1, entry 9), whereas a poor yield is obtained with $Mn(OAc)_3{\cdot}2H_2O$ (Table 1, entry 10), indicating the beneficial effect of the different coordination environment around the Mn(III) center on the catalytic performance. A moderate yield can be obtained at 100 °C also by reducing the catalyst and co-catalyst loading to 0.1 mol%, with a slightly better performance in the presence of PPNBr compared to TBAB (44 and 48% with TBAB and PPNBr, respectively; Table 1 entries 11–12). Under these latter conditions, the catalytic performance of complexes **[MnBrL^{2,3}]** are comparable with respect to **[MnBrL^1]** (48, 50 and 51% yield for **[MnBrL^1]**, **[MnBrL^2]** and **[MnBrL^3]** respectively; Table 1, entries 12–14). Interestingly, all the three complexes **[MnBrL$^{1–3}$]** outperformed the metal precursor $Mn(OAc)_3{\cdot}2H_2O$ (31%, Table 1, entry 15). In all the performed tests, no byproducts were detected, indicating the full selectivity towards the desired product, under the adopted reaction conditions.

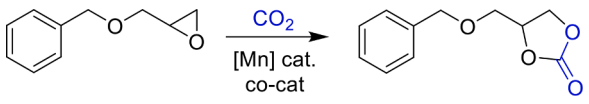

Scheme 3. Model reaction used in this study, cycloaddition between benzyl glycidyl ether (BGE) and CO_2 to form 1-benzylglycerol-2,3-carbonate.

Table 1
Cycloaddition reaction to form 1-benzylglycerol-2,3-carbonate using **[MnBrL$^{1–3}$]** in DMF.

Entry	Catalyst (mol%)[a]	Co-catalyst (mol%)[a]	T / °C	Time / h	Yield[b] /%	TON[c]	TOF[d] / h^{-1}
1	–	–	100	19	0		
2[e]	–	PPNBr (1)	60	19	0		
3		PPNBr (1)	100	19	27		
4	–	PPNBr (0.1)	100	19	9		
5	–	TBAB (0.1)	100	19	13		
6[f]	**[MnBrL^1]** (1)	PPNBr (1)	25	19	3	3	
7[e]	**[MnBrL^1]** (1)	PPNBr (1)	60	19	43	43	2
8	**[MnBrL^1]** (1)	PPNBr (1)	100	19	100	100	5
9	**[MnBrL^1]** (1)	–	100	19	100	100	5
10	$Mn(OAc)_3$ (1)	–	100	19	10	10	1
11	**[MnBrL^1]** (0.1)	TBAB (0.1)	100	19	44	440	23
12	**[MnBrL^1]** (0.1)	PPNBr (0.1)	100	19	48	480	25
13	**[MnBrL^2]** (0.1)	PPNBr (0.1)	100	19	50	500	26
14	**[MnBrL^3]** (0.1)	PPNBr (0.1)	100	19	51	510	27
15	$Mn(OAc)_3$ (0.1)	PPNBr (0.1)	100	19	31	310	16

Reaction conditions: BGE 31.0 mmol in DMF, solvent quantity 1.5 mL, $p(CO_2) = 5$ atm.
[a] mol% with respect to BGE.
[b] Yield determined by ^{1}H NMR using 2,5-dimethylfuran as an internal standard.
[c] Turnover number (TON) calculated as mol of carbonate produced/mol catalyst.
[d] Turnover frequency (TOF) calculated as (TON/reaction time in h).
[e] $p(CO_2) = 3$ atm.
[f] $p(CO_2) = 4$ atm.

Under neat conditions, the catalyzed reaction between BGE and CO_2 showed significantly better performances (Table 2). In fact, a good yield (76%) was obtained with **[MnBrL^1]** (0.1 mol%) and PPNBr (0.1 mol%) at 100 °C for 19 h (Table 2, entry 16), compared to the test using DMF as the solvent (48% yield; Table 1, entry 12). By considering the better performance of the system under neat conditions, we decreased the reaction time from 19 to 7 h in the comparative tests. A series of blank experiments, performed under neat conditions to evaluate once again the effect of the co-catalyst by itself (Table 2, entries 17–22), showed that the contribution of TBAB increased considerably under neat conditions. In fact, when used in 1 mol% with respect to the epoxide, at 100 °C it reached 64% yield in 7 h (Table 2, entry 22). Conversely, low to poor yields were obtained by decreasing the temperature (33, 17 and 5% at 80, 60 and 40 °C, respectively) or the TBAB loading to 0.1 mol% (8% at 100 °C) (Table 2, entries 18–22). We thus tested the catalytic activity of the complexes by using 0.1 mol% of the catalyst and of the co-catalyst, at 100 °C in 7 h, obtaining comparable yields (35, 43 and 49% for **[MnBrL^1]**, **[MnBrL^2]** and **[MnBrL^3]** respectively; Table 2, entries 24–26) to those recorded in DMF under much longer reaction time (19 h,

Table 2
Cycloaddition reaction to form 1-benzylglycerol-2,3-carbonate using **[MnBrL$^{1-3}$]** under neat conditions.

Entry	Catalyst (mol%)[a]	Co-catalyst (mol%)[a]	T/ °C	Time / h	pCO_2/ atm	Yield[b] /%	TON[c]	TOF[d] / h^{-1}
16	**[MnBrL^1]** (0.1)	PPNBr (0.1)	100	19	5	76	760	40
17	–	–	100	7	5	0		
18	–	TBAB (0.1)	100	7	5	8		
19	–	TBAB (1)	40	7	5	5		
20	–	TBAB (1)	60	7	5	17		
21	–	TBAB (1)	80	7	5	33		
22	–	TBAB (1)	100	7	5	64		
23	**[MnBrL^1]** (0.1)	PPNBr (0.1)	100	7	5	35	350	50
24	**[MnBrL^1]** (0.1)	TBAB (0.1)	100	7	5	35	350	50
25	**[MnBrL^2]** (0.1)	TBAB (0.1)	100	7	5	43	430	61
26	**[MnBrL^3]** (0.1)	TBAB (0.1)	100	7	5	49	490	70
27	**[MnBrL^3]** (0.1)	TBAC (0.1)	100	7	5	33	330	47
28	**[MnBrL^3]** (0.1)	TBAI (0.1)	100	7	5	47	470	67
29	**[MnBrL^3]** (0.1)	PPNBr (0.1)	100	7	5	46	460	66
30	**[MnBrL^3]** (0.1)	–	100	7	5	14	140	20
31	**(H_4L^2)Br_2** (0.1)	–	100	7	5	5		
32	**(H_4L^2)Br_2** (0.2)	–	100	7	5	17		
33	**(H_4L^2)Br_2** (0.5)	–	100	7	5	63		
34	$Mn(OAc)_3$ (0.1)	TBAB (0.1)	100	7	5	17	170	24
35	**[MnBrL^3]** (0.1)	TBAB (0.1)	100	7	1[e]	45	450	64
36	**[MnBrL^3]** (0.1)	TBAB (0.1)	100	7	3	47	470	67
37	**[MnBrL^3]** (0.1)	TBAB (0.1)	100	7	7	51	510	73
38	**[MnBrL^3]** (0.1)	TBAB (1)	40	7	5	10	100	14
39	**[MnBrL^3]** (0.1)	TBAB (1)	60	7	5	28	280	40

Reaction conditions: BGE 51.0 mmol under neat conditions, $p(CO_2) = 5$ atm.
[a] mol% with respect to BGE.
[b] Yield determined by ^{1}H NMR using 2,5-dimethylfuran as an internal standard.
[c] Turnover number (TON) calculated as mol of carbonate produced/mol catalyst.
[d] Turnover frequency (TOF) calculated as (TON/reaction time in h).
[e] Balloon.

see Table 1). In this case, the trend of the catalytic performance is **[MnBrL^3]** > **[MnBrL^2]** > **[MnBrL^1]**, with more marked differences among the complexes compared to the tests in the presence of DMF. In the case of complex **[MnBrL^1]**, the same product yield (35%, Table 2, entries 23 and 24) was obtained with TBAB and PPNBr. In addition, complex **[MnBrL^3]** was tested by using tetrabutylammonium chloride (TBAC) and tetrabutylammonium iodide (TBAI) as the co-catalysts, obtaining 33% and 47% yield respectively (Table 2, entries 27 and 28): this clearly indicates that TBAB is the best co-catalyst among the three tested tetrabutylammonium halides. A test was then performed by using complex **[MnBrL^3]** (0.1 mol%) without the co-catalyst, obtaining 14% yield (Table 2, entry 30). The latter experiment supports the presence of a synergistic effect between the catalyst and the co-catalyst. In fact, TBAB (0.1 mol%) by itself reached 8% yield (Table 2, entry 18), but when **[MnBrL^3]** and TBAB were combined (both 0.1 mol%) the yield increased to 49% (Table 2, entry 26). Blank experiments in the presence of the ligand precursor **(H_4L^2)Br_2** at different loading were also carried out (Table 2, entries 31–33). In these cases, the co-catalyst was not added, considering that the bromides are already included in the proligand formula. The obtained product yields are comparable with those found with TBAB alone (Table 2, entries 18, 22), suggesting that for the ligand precursor **(H_4L^2)Br_2** the catalytic performance is ascribable to the bromide anions. Thereafter, we evaluated the CO_2 pressure effect at 100 °C, working with catalyst **[MnBrL^3]** (0.1 mol%) and TBAB (0.1 mol%). The obtained yields, 45, 47, 49, and 51% at 1, 3, 5, and 7 atm respectively (Table 2, entries 26 and 35–37), suggest a slight effect of the CO_2 pressure on the catalytic performance. Finally, we explored the possibility of working at lower temperature, 40 and 60 °C, but low product yields were obtained by using **[MnBrL^3]** (0.1 mol%), even increasing the TBAB loading to 1 mol% (10 and 28% respectively, Table 2, entries 38 and 39).

To gain further insight on the catalyzed reaction between CO_2 and BGE, a kinetic study at different temperatures was performed, by using complex **[MnBrL^3]** as catalyst (0.1 mol%) and TBAB (0.1 mol%) under neat conditions. The product formation versus time was monitored at 100, 90, 80, and 70 °C, by running a series of catalytic tests at different time for each investigated temperature (Fig. 4a). The results of the kinetic experiments, reported in Fig. 4 and in Table S2, show a clear effect of the temperature. After 5 h, the obtained TOF values are in fact 74, 48, 36, and 22 h^{-1} at 100, 90, 80, and 70 °C respectively (Table S2, entries S3, S10, S17, and S22). Under the adopted reaction conditions, a pseudo first order kinetic with respect to BGE was observed. The first order kinetic constants (k_{obs}), obtained by a linear regression of the ln([BGE]/[BGE]$_0$) values versus time (Fig. 4b and Table S2), are $25.0 \cdot 10^{-6}$, $15.6 \cdot 10^{-6}$, $10.0 \cdot 10^{-6}$ and $6.1 \cdot 10^{-6}$ s^{-1} at 100, 90, 80 and 70 °C, respectively. Activation parameters (Table 3) were estimated by employing the Eyring and Arrhenius equations (Fig. 4c and 4d). The obtained activation energy, enthalpy and entropy are E_a = 11.9 kcal·mol^{-1}, $\Delta H^{\ddagger}$ = 11.2 kcal·mol^{-1}, and $\Delta S^{\ddagger}$ = −50 cal·mol^{-1}·K^{-1} respectively (Table 3). The comparison with literature data is not trivial because the kinetic studies reported for this reaction are limited in number and performed with different substrates and co-catalysts. Nevertheless, Gou, Qi *et al.* estimated E_a = 7.1 kcal·mol^{-1} for a binary catalytic system based on a Mn(III) porphyrin derivative and trimethylphenylammonium tribromide (TPAP) and phenylglycidyl ether (PGE) as the substrate [28]. Rehman *et al.* reported E_a = 11.0 kcal·mol^{-1}, $\Delta H^{\ddagger}$ = 10.2 kcal·mol^{-1}, and $\Delta S^{\ddagger}$ = −38 cal·mol^{-1}·K^{-1} for a system based on pyrrolidinopyridinium iodide (PPI) in combination with ZnI_2 and styrene oxide (SO) as co-catalyst and substrate, respectively [73]. Capacchione *et al.* obtained $\Delta H^{\ddagger}$ = 8.4 kcal·mol^{-1} and $\Delta S^{\ddagger}$ = −33 cal·mol^{-1}·K^{-1} for [OSSO]-type iron(III) complexes and TBAB co-catalyst, using propylene oxide (PO) as the substrate [74].

Finally, we tested the CO_2 cycloaddition reaction also with three different epoxides, namely styrene oxide (SO), 1,2-dodecene oxide (DO), and cyclohexene oxide (CO). The yield in the corresponding carbonates (Chart 1), obtained at 100 °C, in 7 h and with **[MnBrL^3]** (0.1 mol%) and TBAB (0.1 mol%) are reported in Table 4. In the case of SO and DO, the observed yields (55 and 44% respectively, Table 4, entries 40 and 43) are comparable with that observed with BGE (49%), under the same conditions. The slightly lower reactivity with DO compared to BGE can

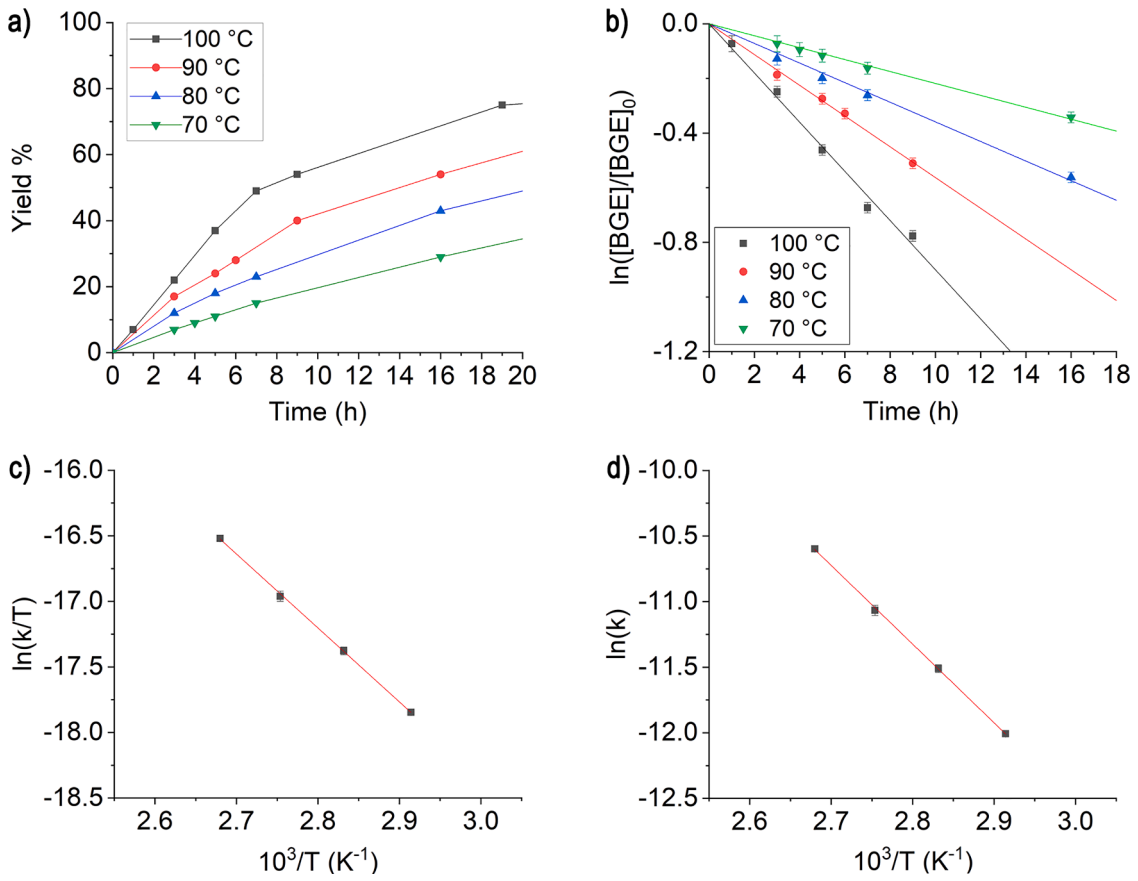

Fig. 4. Kinetic data for catalyst **[MnBrL^3]** in CO_2 cycloaddition to BGE (Tables S2-S5). a) 1-benzylglycerol-2,3-carbonate yields obtained at different temperatures under neat conditions, p(CO_2) = 5 atm, BGE (5.3 mmol), **[MnBrL^3]** (0.1 mol% with respect to BGE), TBAB (0.1 mol% with respect to BGE), lines are only guides for the eyes. b) Semilogarithmic plot of ln[BGE]/[BGE]$_0$ versus time. c) Eyring plot, ln(k/T) versus 1/T. d) Arrhenius plot, ln(k) vs 1/T.

Table 3
Activation parameters estimated by using the Arrhenius and Eyring equations.

E_a (kcal·mol^{-1})	$\Delta H^{\ddagger}$ (kcal·mol^{-1})	$\Delta S^{\ddagger}$ (cal·K^{-1}·mol^{-1})	$\Delta G^{\ddagger}$ (kcal·mol^{-1})[a]
11.9 ± 0.6	11.2 ± 0.5	−50 ± 2	30 ± 1

[a] T = 373.15 K.

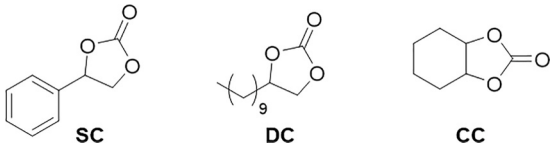

Chart 1. Cyclic carbonates formed in the catalytic tests reported in Table 4. SC = Styrene carbonate, DC = 1,2-dodecene carbonate, CC = cyclohexene carbonate.

be explained with the lower polarity of the reaction medium, as suggested by Capacchione *et al.* [36]. In the case of CO, the expected product is formed, but only in low yield (6%, Table 4, entry 47), as expected for an internal epoxide, for which higher catalyst loading and harsher conditions are usually necessary to reach good product yields [36]. A quantitative product yield can be obtained only by increasing the reaction time to 19 h and the catalyst loading to 0.5 mol% with respect to the substrate in the case of SO, DO and BGE, whereas the yield remains poor with CO (Table 4, entries 42, 45, 46 and 49). Repeated doses of the substrate were performed with BGE, obtaining a quantitative yield also in the second and third run with the same catalytic mixture (Table 4, entries 46), thus suggesting that the catalyst is still active after long reaction time and prolonged heating. At last, we run an experiment with SO, at 60 °C, 24 h, by using **[MnBrL^3]** (0.01 mol%) and TBAB (1 mol%), at 1 atm (Table 4, entry 50), conditions employed by das Chagas and coworkers with Mn(III) porphyrin based catalysts, and the corresponding blank experiment (Table 4, entry 51) [27]. A slightly lower TON was observed with our system (2300), with respect to those of Mn (III) porphyrin catalysts, under the same conditions (2494–3759) [27]. Interestingly, in the case of the Mn(III) porphyrin based catalysts, the observed TON are strongly related to the apical ligand present in the square pyramidal complex structure, being the bromide and the iodate derivatives the least (2494 TON) and the most (3797 TON) active [27].

3.3. Computational studies

The catalytic mechanism was explored at ZORA-OPBE/TZ2P level of theory, choosing the fragments with L^2 and L^3; ethylene oxide (**EO**) and styrene oxide (**SO**) were used as substrates. The geometries of **[MnBrL^2]** and **[MnBrL^3]** were fully optimized in quintet state. Any attempt of coordinating the **EO**/**SO** substrate to the **[MnBrL^{2,3}]** complex failed. Conversely, binding of the epoxide was observed if the Br^- ligand in axial position is removed. Thus, we have identified ^{5}**[Mn(EO)L^{2,3}]**$^+$, generated upon bromide substitution with epoxide, as the real catalyst in the cycle, in agreement with the observation by das Chagas and coworkers [27] on Mn(III) porphyrin catalyzed process, which indicates that the lability of the axial ligand is favorable for the reaction. By chance, the lability of the bromide ligand was experimentally confirmed in our system by the obtainment of complex **[MnClL^3]** by treating a CH_2Cl_2 solution of the bromido complex with brine. We have sketched a model catalytic mechanism in Scheme 4 and optimized all the intermediates and transition states (Fig. 5) for the three main steps, i.e.

Table 4
Cycloaddition reaction with different epoxides under neat conditions.

Entry	Epoxide	Catalyst (mol%)[a]	Co-catalyst (mol%)[a]	T / °C	Time / h	p(CO_2) / atm	Yield[b] /%	TON[c]	TOF[d] / h^{-1}
40	**SO**	**[MnBrL^3]** (0.1)	TBAB (0.1)	100	7	5	55	550	79
41	**SO**	**[MnBrL^3]** (0.1)	TBAB (0.1)	100	19	5	82	820	43
42	**SO**	**[MnBrL^3]** (0.5)	TBAB (0.1)	100	19	5	100	200	11
43	**DO**	**[MnBrL^3]** (0.1)	TBAB (0.1)	100	7	5	44	440	63
44	**DO**	**[MnBrL^3]** (0.1)	TBAB (0.1)	100	19	5	52	520	27
45	**DO**	**[MnBrL^3]** (0.5)	TBAB (0.1)	100	19	5	100	200	11
46	**BGE**	**[MnBrL^3]** (0.5)	TBAB (0.1)	100	19	5	100 (100)[e] (100)[f]	200	11
47	**CO**	**[MnBrL^3]** (0.1)	TBAB (0.1)	100	7	5	6	60	9
48	**CO**	**[MnBrL^3]** (0.1)	TBAB (0.1)	100	19	5	8	80	4
49	**CO**	**[MnBrL^3]** (0.5)	TBAB (0.1)	100	19	5	13	26	1
50	**SO**	**[MnBrL^3]** (0.01)	TBAB (1)	60	24	1[g]	23	2300	96
51	**SO**	–	TBAB (1)	60	24	1[g]	14		

Reaction conditions: Epoxide 51.0 mmol under neat conditions, T = 100 °C, SO = Styrene oxide, DO = 1,2-dodecene oxide, CO = Cyclohexene oxide.
[a] mol% with respect to the epoxide.
[b] Yield determined by ^{1}H NMR using 2,5-dimethylfuran as an internal standard.
[c] Turnover number (TON) calculated as mol of carbonate produced/mol catalyst.
[d] Turnover frequency (TOF) calculated as (TON/reaction time in h).
[e] second run performed by adding substrate (51.0 mmol) to the same reaction mixture.
[f] third run performed by adding substrate (51.0 mmol) to the same reaction mixture.
[g] Balloon.

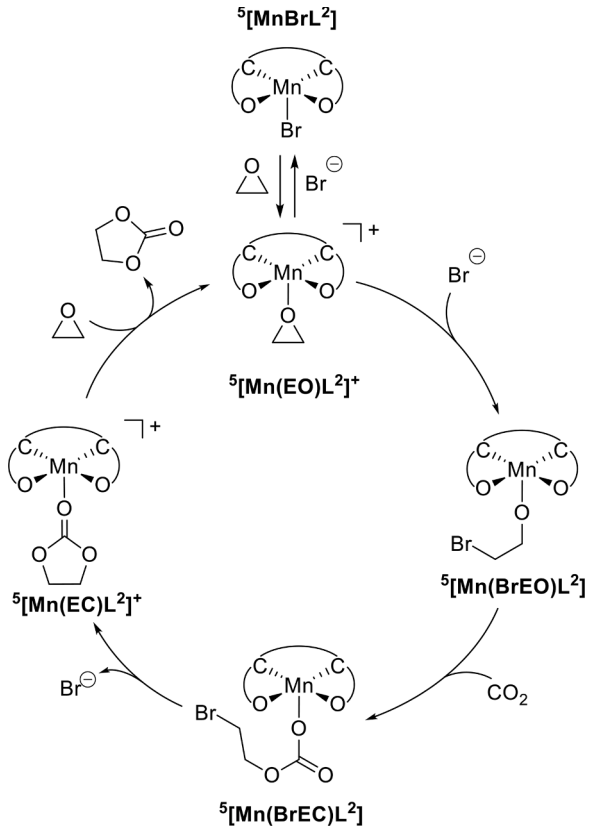

Scheme 4. Proposed reaction mechanism for the **[Mn(EO)L^2]**$^+$ catalyzed cycloaddition of ethylene oxide (**EO**) with CO_2.

nucleophilic attack of the bromide anion followed by ring opening giving ^{5}**[Mn(B*r*EO)L^2]**, CO_2 insertion into the Mn-O bond, thus affording ^{5}**[Mn(B*r*EC)L^2]**, and finally formation of the cyclic carbonate with the bromide anion cleavage, obtaining ^{5}**[Mn(EC)L^2]**$^+$. It is important to mention that an alternative mechanism was reported in literature for a similar manganese catalyzed reaction, in which after the formation of ^{5}**[Mn(B*r*EO)L^2]**, instead of having the CO_2 insertion leading to ^{5}**[Mn(B*r*EC)L^2]**, the nucleophilic alkoxy group of the complex attacks the electrophilic carbon of CO_2 generating a different carbonate intermediate ^{5}**[Mn(BrCH$_2$CH$_2$OCOO$^-$)L^2]** (O represents the donor atom of the fragment) [28]. However, any attempt to optimize this alternative intermediate was unsuccessful; thus, in our system, the reaction is supposed to proceed via CO_2 insertion into the Mn-O bond.

The carbonation is the slowest step of the whole path; it is slightly energetically unfavored (+2.95 kcal·mol^{-1}) and has an activation energy of 62.54 kcal·mol^{-1}, which is approximately almost twice and three times higher than those of the preceding and following step, i.e. 37.30 and 22.84 kcal·mol^{-1}, respectively. No attempt was done to ameliorate the energetics, like location of reactant and product complexes along the potential energy surface (PES) or addition of ions to neutralize the total charge. Based on this model, the carbonation is identified as the slow step for Mn(III) catalyzed CO_2 cycloaddition to epoxides. Focusing on the reaction energy of this step, we have investigated the effect of replacing the carbene ligand **L^2** with **L^3**. Particularly, the effect of using ^{5}**[MnL^3]**$^+$ combined to EO makes the step more energetically favored (−1.44 kcal·mol^{-1}). This finding is in agreement with trend in the catalytic efficiency observed experimentally under neat conditions (**[MnBrL^3] > [MnBrL^2] > [MnBrL^1]**) with BGE as substrate. Subsequently, we also evaluated the effect of the substrate, by using SO. By replacing EO with SO, the carbonation step is energetically favored with ^{5}**[MnL^2]**$^+$ (−1.87 kcal·mol^{-1}), although, with ^{5}**[MnL^3]**$^+$ the same step is unfavored (+3.69 kcal·mol^{-1}). We speculate that this different trend is possibly due to the increased steric hindrance of the substrate

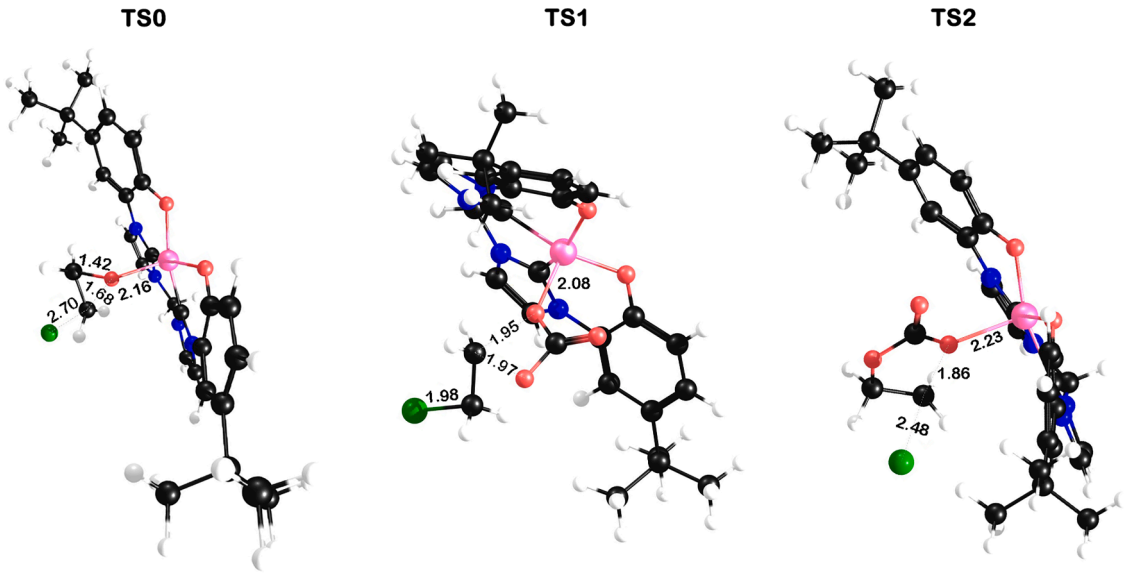

Fig. 5. Optimized geometries of the transition states along the catalyzed path shown in Scheme 4; level of theory: ZORA-OPBE/TZ2P. Selected interatomic distances (Å) are shown. ^{5}[**Mn**(EO)L^2]$^+$ to ^{5}[Mn(BrEO)L^2] = **TS0;** ^{5}[Mn(BrEO)L^2] to ^{5}[Mn(BrEC)L^2] = **TS1;** ^{5}[Mn(BrEC)L^2] to ^{5}[**Mn**(EC)L^2]$^+$ = TS2.

compared to EO.

4. Conclusion

The synthesis of three bis(NHC)-bis(phenolate) (OˆCˆCˆO) ligand precursors and of their corresponding manganese(III) complexes **[MnBrL$^{1-3}$]** was successfully accomplished and optimized. The multi-step procedure is characterized by high yields in every step, except for the imidazole derivative synthesis (yield ca. 50%). The organometallic complexes were fully characterized and the crystallographic structures of **[MnBrL^1(MeOH)]** and **[MnBrL^3]** were determined. The solvento complex **[MnBrL^1(MeOH)]** represents the first example of a distorted octahedral manganese(III) complex with NHC ligands. The prepared complexes are active homogeneous catalysts in the cycloaddition of benzyl glycidyl ether with CO_2 to obtain the corresponding cyclic carbonate. The metal complexes are used in a binary catalytic system together with a bromide source (PPNBr or TBAB) as co-catalyst in 1:1 ratio. In this frame, the synergistic cooperation between the metal catalyst and the co-catalyst was confirmed. Under the adopted catalytic conditions, a complete selectivity towards the desired cyclic carbonate was observed, and no further products or byproducts were detected. The reaction was carried out both in DMF solution and under neat conditions, with the latter showing significantly better performances. A ligand effect on the catalytic activity of the complexes has been observed, with the performance trend **[MnBrL^3]** > **[MnBrL^2]** > **[MnBrL^1]** found under neat conditions. The kinetic study performed on the reaction catalyzed by **[MnBrL^3]** showed a pseudo first order kinetic law in the product formation, with estimated activation parameters $\Delta H^{\ddagger} = 11.2 \pm 0.5$ kcal·mol^{-1} and $\Delta S^{\ddagger} = -50 \pm 2$ cal·mol^{-1}·K^{-1}. These data are consistent with those reported in the literature for similar catalytic systems [28,73,74]. Concerning the investigation of the reaction mechanism by DFT calculations, the first important insight is that coordination of the epoxide to the starting complex to form a hexacoordinated species is not favored. Thus, the substitution of the bromide ligand by the epoxide is supposed to be the first step of the mechanism, with the species [Mn(EO)L]$^+$ being the active form of the catalyst. The CO_2 insertion has been identified as the rate determining step, nicely in agreement with the negative activation entropy variation found with the Eyring plot. The energy profiles calculated with the model substrate EO also suggest a lower activation energy for the [MnL^3]$^+$ system compared to the [MnL^2]$^+$ one, confirming the trend observed experimentally. The reaction scope was thus investigated using the most active **[MnBrL^3]** catalyst, and good yields were obtained with a low catalyst loading (0.1 mol%), also with challenging substrates such as 1,2-dodecene oxide. Tests performed under the same conditions reported in the literature for porphyrin-based Mn(III) catalysts, indicate a slightly lower performance of our complexes with the benchmark substrate styrene oxide [27]. However, considering that the present work is the first report on the catalytic activity of Mn(III) complexes with OˆCˆCˆO ligands in the cycloaddition of epoxides with CO_2, further optimization of the molecular structure of the catalysts is expected to increase the catalytic performance.

Funding

This work was supported by the Department of Chemical Sciences of the University of Padova [P-DiSC#01BIRD2019-UNIPD].

CRediT authorship contribution statement

Giammarco Meloni: Investigation, Data curation, Writing – original draft, Writing – review & editing. **Luca Beghetto:** Investigation, Data curation, Writing – original draft, Writing – review & editing. **Marco Baron:** Conceptualization, Resources, Data curation, Writing – review & editing, Supervision, Funding acquisition. **Andrea Biffis:** Data curation, Writing – review & editing. **Paolo Sgarbossa:** Investigation, Resources, Data curation, Writing – review & editing. **Miriam Mba:** Data curation, Writing – review & editing, Funding acquisition. **Paolo Centomo:** Data curation, Writing – review & editing, Funding acquisition. **Laura Orian:** Investigation, Data curation, Writing – original draft, Writing – review & editing. **Claudia Graiff:** Investigation, Resources, Writing – review & editing. **Cristina Tubaro:** Conceptualization, Resources, Writing – review & editing, Supervision.

Declaration of Competing Interest

The authors declare that they have no known competing financial interests or personal relationships that could have appeared to influence the work reported in this paper.

Data availability

Data will be made available on request.

Supplementary materials

Supplementary material associated with this article can be found, in the online version, at doi:10.1016/j.mcat.2023.113006.

References

[1] P. Pfeiffer, E. Breith, E. Lübbe, T. Tsumaki, Tricyclische orthokondensierte Nebenvalenzringe, Justus Liebigs Ann. Chem. 503 (1933) 84–130, https://doi.org/10.1002/jlac.19335030106.

[2] W. Zhang, J.L. Loebach, S.R. Wilson, E.N. Jacobsen, Enantioselective epoxidation of unfunctionalized olefins catalyzed by salen manganese complexes, J. Am. Chem. Soc. 112 (1990) 2801–2803, https://doi.org/10.1021/ja00163a052.

[3] K. Srinivasan, P. Michaud, J.K. Kochi, Epoxidation of olefins with cationic (salen) manganese(III) complexes. The modulation of catalytic activity by substituents, J. Am. Chem. Soc. 108 (1986) 2309–2320, https://doi.org/10.1021/ja00269a029.

[4] T. Katsuki, Catalytic asymmetric oxidations using optically active (salen) manganese(III) complexes as catalysts, Coord. Chem. Rev. 140 (1995) 189–214, https://doi.org/10.1016/0010-8545(94)01124-T.

[5] E.Y. Tshuva, I. Goldberg, M. Kol, Isospecific Living Polymerization of 1-Hexene by a Readily Available Nonmetallocene C2-Symmetrical Zirconium Catalyst, J. Am. Chem. Soc. 122 (2000) 10706–10707, https://doi.org/10.1021/ja001219g.

[6] C.J. Whiteoak, R. Torres Martin de Rosales, A.J.P. White, G.J.P. Britovsek, Iron(II) Complexes with Tetradentate Bis(aminophenolate) Ligands: Synthesis and Characterization, Solution Behavior, and Reactivity with O2, Inorg. Chem. 49 (2010) 11106–11117, https://doi.org/10.1021/ic1016998.

[7] K.C. Gupta, A.K. Sutar, Catalytic activities of Schiff base transition metal complexes, Coord. Chem. Rev. 252 (2008) 1420–1450, https://doi.org/10.1016/j.ccr.2007.09.005.

[8] N. Nakata, T. Toda, A. Ishii, Recent advances in the chemistry of Group 4 metal complexes incorporating [OSSO]-type bis(phenolato) ligands as post-metallocene catalysts, Polym. Chem. 2 (2011) 1597–1610, https://doi.org/10.1039/C1PY00058F.

[9] V. Paradiso, V. Capaccio, D.H. Lamparelli, C. Capacchione, [OSSO]-bisphenolate metal complexes: A powerful and versatile tool in polymerization catalysis, Coord. Chem. Rev. 429 (2021) 213644–213684, https://doi.org/10.1016/j.ccr.2020.213644.

[10] R.J. Long, D.J. Jones, V.C. Gibson, A.J.P. White, Zirconium Complexes Containing Tetradentate O,P,P,O Ligands: Ethylene and Propylene Polymerization Studies, Organometallics 27 (2008) 5960–5967. https://doi.org/10.1021/om800652w.

[11] T. Yagyu, K. Yano, T. Kimata, K. Jitsukawa, Synthesis and Characterization of a Manganese(III) Complex with a Tetradentate N-Heterocyclic Carbene Ligand, Organometallics 28 (2009) 2342–2344, https://doi.org/10.1021/om900007b.

[12] R. Kunert, C. Philouze, O. Jarjayes, F. Thomas, Stable M(II)-Radicals and Nickel(III) Complexes of a Bis(phenol) N-Heterocyclic Carbene Chelated to Group 10 Metal Ions, Inorg. Chem. 58 (2019) 8030–8044, https://doi.org/10.1021/acs.inorgchem.9b00784.

[13] K. Li, G. Cheng, C. Ma, X. Guan, W.-.M. Kwok, Y. Chen, W. Lu, C.-.M. Che, Light-emitting platinum(II) complexes supported by tetradentate dianionic bis(N-heterocyclic carbene) ligands: towards robust blue electrophosphors, Chem. Sci. 4 (2013) 2630–2644, https://doi.org/10.1039/C3SC21822H.

[14] M.N. Hopkinson, C. Richter, M. Schedler, F. Glorius, An overview of N-heterocyclic carbenes, Nature 510 (2014) 485–496, https://doi.org/10.1038/nature13384.

[15] S. Hameury, P. de Frémont, P. Braunstein, Metal complexes with oxygen-functionalized NHC ligands: synthesis and applications, Chem. Soc. Rev. 46 (2017) 632–733, https://doi.org/10.1039/C6CS00499G.

[16] M. Baron, E. Battistel, C. Tubaro, A. Biffis, L. Armelao, M. Rancan, C. Graiff, Single-Step Synthesis of Dinuclear Neutral Gold(I) Complexes with Bridging Di(N-heterocyclic carbene) Ligands and Their Catalytic Performance in Cross Coupling Reactions and Alkyne Hydroamination, Organometallics 37 (2018) 4213–4223, https://doi.org/10.1021/acs.organomet.8b00531.

[17] M. Baron, C. Tubaro, M.L.C. Cairoli, L. Orian, S. Bogialli, M. Basato, M.M. Natile, C. Graiff, Gold(III) Bis(di-N-heterocyclic carbene) square planar trication with axial ligand interactions with bromides from Ag/Br counteranion assemblies, Organometallics 36 (2017) 2285–2292, https://doi.org/10.1021/acs.organomet.7b00163.

[18] M. Baron, A. Dall'Anese, C. Tubaro, L. Orian, V. Di Marco, S. Bogialli, C. Graiff, M. Basato, A square planar gold(iii) bis-(1,1′-dimethyl-3,3′-methylene-diimidazol-2,2′-diylidene) trication as an efficient and selective receptor towards halogen anions: the cooperative effect of Au···X and X···HC interactions Structural and Luminescent Properties of Homoleptic Silver(I), Gold(I), and Palladium(II) Complexes with nNHC-tzNHC Heteroditopic Carbene Ligands, Dalton Trans 47 (2018) 935–945, https://doi.org/10.1039/c7dt03672h.

[19] V. Stoppa, T. Scattolin, M. Bevilacqua, M. Baron, C. Graiff, L. Orian, A. Biffis, I. Menegazzo, M. Roverso, S. Bogialli, F. Visentin, C. Tubaro, Mononuclear and dinuclear gold(I) complexes with a caffeine-based di(N-heterocyclic carbene) ligand: synthesis, reactivity and structural DFT analysis, New J. Chem. 45 (2021) 961–971, https://doi.org/10.1039/D0NJ05906D.

[20] S. Bellemin-Laponnaz, R. Welter, L. Brelot, S. Dagorne, Synthesis and structure of V (V) and Mn(III) NHC complexes supported by a tridentate bis-aryloxide-N-heterocyclic carbene ligand, J. Organomet. Chem. 694 (2009) 604–606, https://doi.org/10.1016/j.jorganchem.2008.12.049.

[21] S.M.P. Vanden Broeck, C.S.J. Cazin, Manganese-N-heterocyclic carbene (NHC) complexes – An overview, Polyhedron 205 (2021), 115204, https://doi.org/10.1016/j.poly.2021.115204.

[22] J. Agarwal, T.W. Shaw, C.J. Stanton III, G.F. Majetich, A.B. Bocarsly, H. F. Schaefer III, NHC-Containing Manganese(I) Electrocatalysts for the Two-Electron Reduction of CO2, Angew. Chem. Int. Ed. 53 (2014) 5152–5155, https://doi.org/10.1002/anie.201311099.

[23] M. Pinto, S. Friães, F. Franco, J. Lloret-Fillol, B. Royo, Manganese N-Heterocyclic Carbene Complexes for Catalytic Reduction of Ketones with Silanes, ChemCatChem 10 (2018) 2734–2740, https://doi.org/10.1002/cctc.201800241.

[24] A. Das, S. Charan Mandal, B. Pathak, Unraveling the catalytically preferential pathway between the direct and indirect hydrogenation of CO_2 to CH_3OH using N-heterocyclic carbene-based Mn(i)catalysts: a theoretical approach, Catal. Sci. Technol. 11 (2021) 1375–1385, https://doi.org/10.1039/D0CY02064H.

[25] S. Friães, S. Realista, C.S.B. Gomes, P.N. Martinho, L.F. Veiros, M. Albrecht, B. Royo, Manganese Complexes With Chelating and Bridging Di-Triazolylidene ligands: Synthesis and Reactivity, Dalton Trans. 50 (2021) 5911–5920. https://doi.org/10.1039/D1DT00444A.

[26] S.C.A. Sousa, S. Realista, B. Royo, Bench-Stable Manganese NHC Complexes for the Selective Reduction of Esters to Alcohols with Silanes, Adv. Synth. Catal. 362 (2020) 2437–2443, https://doi.org/10.1002/adsc.202000148.

[27] J.L.S. Milani, A.M. Meireles, W.A. Bezerra, Dayse.C.S. Martins, D. Cangussu, R. P. das Chagas, MnIII Porphyrins: Catalytic Coupling of Epoxides with CO_2 under Mild Conditions and Mechanistic Considerations, ChemCatChem 11 (2019) 4393–4402, https://doi.org/10.1002/cctc.201900745.

[28] X. Jiang, F. Gou, C. Qi, C2v-symmetric metalloporphyrin promoted cycloaddition of epoxides with CO_2 under atmospheric pressure, J. CO2 Util. 29 (2019) 134–139, https://doi.org/10.1016/j.jcou.2018.12.003.

[29] J.L.S. Milani, A.M. Meireles, B.N. Cabral, W. de Almeida Bezerra, F.T. Martins, D. C. da Silva Martins, R.P. das Chagas, Highly active Mn(III) meso-tetrakis(2,3-dichlorophenyl)porphyrin catalysts for the cycloaddition of CO2 with epoxides, J. CO2 Util. 30 (2019) 100–106, https://doi.org/10.1016/j.jcou.2018.12.017.

[30] B.N. Cabral, J.L.S. Milani, A.M. Meireles, D.C. da Silva Martins, S.L. da Silva Ribeiro, J.S. Rebouças, C.L. Donnici, R.P. das Chagas, Mn(iii)–porphyrin catalysts for the cycloaddition of CO_2 with epoxides at atmospheric pressure: effects of Lewis acidity and ligand structure, New J. Chem. 45 (2021) 1934–1943, https://doi.org/10.1039/D0NJ05280A.

[31] P. Ramidi, C.M. Felton, B.P. Subedi, H. Zhou, Z.R. Tian, Y. Gartia, B.S. Pierce, A. Ghosh, Synthesis and characterization of manganese(III) and high-valent manganese-oxo complexes and their roles in conversion of alkenes to cyclic carbonates, J. CO_2 Util. 9 (2015) 48–57, https://doi.org/10.1016/j.jcou.2014.12.004.

[32] J.Castilla L.Cuesta-Aluja, A.M. Masdeu-Bultó, C.A. Henriques, M.J.F. Calvete, M. M. Pereira, Halogenated meso-phenyl Mn(III) porphyrins as highly efficient catalysts for the synthesis of polycarbonates and cyclic carbonates using carbon dioxide and epoxides, J. Mol. Catal. A Chem. 423 (2016) 489–494, https://doi.org/10.1016/j.molcata.2015.10.025.

[33] P.P. Pescarmona, Cyclic carbonates synthesised from CO_2: Applications, challenges and recent research trends, Curr. Opin. Green Sustain. Chem. 29 (2021), 100457, https://doi.org/10.1016/j.cogsc.2021.100457.

[34] A.W. Kleij, Advancing halide-free catalytic synthesis of CO2-based heterocycles, Curr. Opin. Green Sustain. Chem. 24 (2020) 72–81, https://doi.org/10.1016/j.cogsc.2020.04.002.

[35] F.Della Monica, A. Buonerba, C. Capacchione, Homogeneous Iron Catalysts in the Reaction of Epoxides with Carbon Dioxide, Adv. Synth. Catal. 361 (2019) 265–282, https://doi.org/10.1002/adsc.201801281.

[36] F.Della Monica, A. Buonerba, V. Paradiso, S. Milione, A. Grassi, C. Capacchione, [OSSO]-Type Fe(III) Metallate as Single-Component Catalyst for the CO_2 Cycloaddition to Epoxides, Adv. Synth. Catal. 361 (2019) 283–288, https://doi.org/10.1002/adsc.201801240.

[37] E.Y. Seong, J.H. Kim, N.H. Kim, K.-.H. Ahn, E.J. Kang, Multifunctional and Sustainable Fe-Iminopyridine Complexes for the Synthesis of Cyclic Carbonates, ChemSusChem 12 (2019) 409–415, https://doi.org/10.1002/cssc.201802563.

[38] A.J. Kamphuis, F. Milocco, L. Koiter, P.P. Pescarmona, E. Otten, Highly Selective Single-Component Formazanate Ferrate(II) Catalysts for the Conversion of CO_2 into Cyclic Carbonates, ChemSusChem 12 (2019) 3635–3641, https://doi.org/10.1002/cssc.201900740.

[39] K.A. Andrea, E.D. Butler, T.R. Brown, T.S. Anderson, D. Jagota, C. Rose, E.M. Lee, S.D. Goulding, J.N. Murphy, F.M. Kerton, C.M. Kozak, Iron Complexes for Cyclic Carbonate and Polycarbonate Formation: Selectivity Control from Ligand Design and Metal-Center Geometry, Inorg. Chem. 58 (2019) 11231–11240, https://doi.org/10.1021/acs.inorgchem.9b01909.

[40] J. Liu, G. Yang, Y. Liu, D. Zhang, X. Hu, Z. Zhang, Efficient conversion of CO_2 into cyclic carbonates at room temperature catalyzed by Al-salen and imidazolium hydrogen carbonate ionic liquids, Green Chem. 22 (2020) 4509–4515, https://doi.org/10.1039/D0GC00458H.

[41] G. Fiorani, M. Stuck, C. Martín, M.M. Belmonte, E. Martin, E.C. Escudero-Adán, A. W. Kleij, Catalytic Coupling of Carbon Dioxide with Terpene Scaffolds: Access to Challenging Bio-Based Organic Carbonates, ChemSusChem 9 (2016) 1304–1311, https://doi.org/10.1002/cssc.201600238.

[42] A. Decortes, A.M. Castilla, A.W. Kleij, Salen-Complex-Mediated Formation of Cyclic Carbonates by Cycloaddition of CO_2 to Epoxides, Angew. Chem. Int. Ed. 49 (2010) 9822–9837, https://doi.org/10.1002/anie.201002087.
[43] D.J. Darensbourg, Making Plastics from Carbon Dioxide: Salen Metal Complexes as Catalysts for the Production of Polycarbonates from Epoxides and CO_2, Chem. Rev. 107 (2007) 2388–2410, https://doi.org/10.1021/cr068363q.
[44] F.D. Bobbink, D. Vasilyev, M. Hulla, S. Chamam, F. Menoud, G. Laurenczy, S. Katsyuba, P.J. Dyson, Intricacies of Cation–Anion Combinations in Imidazolium Salt-Catalyzed Cycloaddition of CO_2 Into Epoxides, ACS Catal. 8 (2018) 2589–2594, https://doi.org/10.1021/acscatal.7b04389.
[45] A.J. Kamphuis, F. Picchioni, P.P. Pescarmona, CO_2 -fixation into cyclic and polymeric carbonates: principles and applications, Green Chem. 21 (2019) 406–448, https://doi.org/10.1039/C8GC03086C.
[46] M. Alves, B. Grignard, R. Mereau, C. Jerome, T. Tassaing, C. Detrembleur, Organocatalyzed coupling of carbon dioxide with epoxides for the synthesis of cyclic carbonates: catalyst design and mechanistic studies, Catal. Sci. Technol. 7 (2017) 2651–2684, https://doi.org/10.1039/C7CY00438A.
[47] M. Cokoja, M.E. Wilhelm, M.H. Anthofer, W.A. Herrmann, F.E. Kühn, Synthesis of Cyclic Carbonates from Epoxides and Carbon Dioxide by Using Organocatalysts, ChemSusChem 8 (2015) 2436–2454, https://doi.org/10.1002/cssc.201500161.
[48] J. Liang, Y.-.B. Huang, R. Cao, Metal–organic frameworks and porous organic polymers for sustainable fixation of carbon dioxide into cyclic carbonates, Coord. Chem. Rev. 378 (2019) 32–65, https://doi.org/10.1016/j.ccr.2017.11.013.
[49] S. Singh Dhankhar, B. Ugale, C.M. Nagaraja, Co-Catalyst-Free Chemical Fixation of CO2 into Cyclic Carbonates by using Metal-Organic Frameworks as Efficient Heterogeneous Catalysts, Chem. – Asian J. 15 (2020) 2403–2427. https://doi.org/10.1002/asia.202000424.
[50] K. Epp, A.L. Semrau, M. Cokoja, R.A. Fischer, Dual Site Lewis-Acid Metal-Organic Framework Catalysts for CO2 Fixation: Counteracting Effects of Node Connectivity, Defects and Linker Metalation, ChemCatChem 10 (2018) 3506–3512, https://doi.org/10.1002/cctc.201800336.
[51] K. Huang, J.-.Y. Zhang, F. Liu, S. Dai, Synthesis of Porous Polymeric Catalysts for the Conversion of Carbon Dioxide, ACS Catal. 8 (2018) 9079–9102, https://doi.org/10.1021/acscatal.8b02151.
[52] C. Calabrese, L.F. Liotta, F. Giacalone, M. Gruttadauria, C. Aprile, Supported Polyhedral Oligomeric Silsesquioxane-Based (POSS) Materials as Highly Active Organocatalysts for the Conversion of CO2, ChemCatChem 11 (2019) 560–567, https://doi.org/10.1002/cctc.201801351.
[53] G.M. Sheldrick, SHELXT – Integrated space-group and crystal-structure determination, Acta Crystallogr. Sect. Found. Adv. 71 (2015) 3–8, https://doi.org/10.1107/S2053273314026370.
[54] G.M. Sheldrick, Crystal structure refinement with SHELXL, Acta Crystallogr. Sect. C Struct. Chem. 71 (2015) 3–8, https://doi.org/10.1107/S2053229614024218.
[55] O.V. Dolomanov, L.J. Bourhis, R.J. Gildea, J.a.K. Howard, H. Puschmann, OLEX2: a complete structure solution, refinement and analysis program, J. Appl. Crystallogr. 42 (2009) 339–341, https://doi.org/10.1107/S0021889808042726.
[56] E.J. Baerends, D.E. Ellis, P. Ros, Self-consistent molecular Hartree—Fock—Slater calculations I. The computational procedure, Chem. Phys. 2 (1973) 41–51, https://doi.org/10.1016/0301-0104(73)80059-X.
[57] G. te Velde, F.M. Bickelhaupt, E.J. Baerends, C. Fonseca Guerra, S.J.A. van Gisbergen, J.G. Snijders, T. Ziegler, Chemistry with ADF, J. Comput. Chem. 22 (2001) 931–967, https://doi.org/10.1002/jcc.1056.
[58] ADF 2019.3, SCM, Theoretical Chemistry, Vrije Universiteit, Amsterdam, The Netherlands, http://www.scm.com.
[59] M. Swart, A.W. Ehlers, K. Lammertsma, Performance of the OPBE exchange-correlation functional, Mol. Phys. 102 (2004) 2467–2474, https://doi.org/10.1080/00268970420002750 17.
[60] E. van Lenthe, E.J. Baerends, J.G. Snijders, Relativistic total energy using regular approximations, J. Chem. Phys. 101 (1994) 9783–9792, https://doi.org/10.1063/1.467943.
[61] F. Zaccaria, L.P. Wolters, C.Fonseca Guerra, L. Orian, Insights on selenium and tellurium diaryldichalcogenides: A benchmark DFT study, J. Comput. Chem. 37 (2016) 1672–1680, https://doi.org/10.1002/jcc.24383.
[62] S. Scuppa, L. Orian, A. Donoli, S. Santi, M. Meneghetti, Anti-Kasha's Rule Fluorescence Emission in (2-Ferrocenyl)indene Generated by a Twisted Intramolecular Charge-Transfer (TICT) Process, J. Phys. Chem. A. 115 (2011) 8344–8349, https://doi.org/10.1021/jp2021227.
[63] S. Santi, C. Durante, A. Donoli, A. Bisello, L. Orian, P. Ganis, A. Ceccon, F. Benetollo, Intervalence Charge Transfer in Cationic Heterotrinuclear Fe(III)−Rh(I)−Cr(0) Triads of the Polyaromatic Cyclopentadienyl−Indenyl Ligand, Organometallics 29 (2010) 2046–2053, https://doi.org/10.1021/om900903e.
[64] L. Orian, W.-.J. van Zeist, F.M. Bickelhaupt, Linkage Isomerism of Nitriles in Rhodium Half-Sandwich Metallacycles, Organometallics 27 (2008) 4028–4030, https://doi.org/10.1021/om8004614.
[65] A.D. Becke, A multicenter numerical integration scheme for polyatomic molecules, J. Chem. Phys. 88 (1988) 2547–2553, https://doi.org/10.1063/1.454033.
[66] M. Franchini, P.H.T. Philipsen, L. Visscher, The Becke Fuzzy Cells Integration Scheme in the Amsterdam Density Functional Program Suite, J. Comput. Chem. 34 (2013) 1819–1827, https://doi.org/10.1002/jcc.23323.
[67] P.-.J. Huang, H. Miyasaka, Canting angle dependence of single-chain magnet behaviour in chirality-introduced antiferromagnetic chains of acetate-bridged manganese(iii) salen-type complexes, Dalton Trans. 49 (2020) 16970–16978, https://doi.org/10.1039/D0DT03615C.
[68] a)H. Kooijman, A.L. Spek, M.D. Godbole, E. Bouwman, J. Reedijk, CCDC 654332: Exp. Cryst. Struct. Determin., (2008). https://doi.org/10.5517/CCPYWHZ;. b)A. Collins, E. Brechin, CCDC 1417768: Experimental Crystal Structure Determination, (2015). https://doi.org/10.5517/CC1JL9GW.
[69] J. Hilf, A. Phillips, H. Frey, Poly(carbonate) copolymers with a tailored number of hydroxyl groups from glycidyl ethers and CO_2, Polym. Chem. 5 (2013) 814–818, https://doi.org/10.1039/C3PY00977G.
[70] J. Liu, W. Ren, X. Lu, Fully degradable brush polymers with polycarbonate backbones and polylactide side chains, Sci. China Chem. 58 (2015) 999–1004, https://doi.org/10.1007/s11426-014-5263-z.
[71] J. Geschwind, H. Frey, Poly(1,2-glycerol carbonate): A Fundamental Polymer Structure Synthesized from CO_2 and Glycidyl Ethers, Macromolecules 46 (2013) 3280–3287, https://doi.org/10.1021/ma400090m.
[72] H. Zhang, M.W. Grinstaff, Synthesis of Atactic and Isotactic Poly(1,2-glycerol carbonate)s: Degradable Polymers for Biomedical and Pharmaceutical Applications, J. Am. Chem. Soc. 135 (2013) 6806–6809, https://doi.org/10.1021/ja402558m.
[73] A. Rehman, V.C. Eze, M.F.M.G. Resul, A. Harvey, Kinetics and mechanistic investigation of epoxide/CO_2 cycloaddition by a synergistic catalytic effect of pyrrolidinopyridinium iodide and zinc halides, J. Energy Chem. 37 (2019) 35–42, https://doi.org/10.1016/j.jechem.2018.11.017.
[74] F.Della Monica, B. Maity, T. Pehl, A. Buonerba, A. De Nisi, M. Monari, A. Grassi, B. Rieger, L. Cavallo, C. Capacchione, [OSSO]-Type Iron(III) Complexes for the Low-Pressure Reaction of Carbon Dioxide with Epoxides: Catalytic Activity, Reaction Kinetics, and Computational Study, ACS Catal. 8 (2018) 6882–6893, https://doi.org/10.1021/acscatal.8b01695.